Catalysis Communications 15 (2011) 1–5

Contents lists available at ScienceDirect

Catalysis Communications

journal homepage: www.elsevier.com/locate/catcom

Short Communication

Sol–gel derived V_2O_5–TiO_2 mesoporous materials as catalysts for the total oxidation of chlorobenzene

Chiraz Gannoun [a,*], Romain Delaigle [b], Pierre Eloy [b], Damien P. Debecker [b], Abdelhamid Ghorbel [a], Eric M. Gaigneaux [b]

[a] Laboratoire de Chimie des Matériaux et Catalyse, Département de Chimie, Faculté des Sciences de Tunis, Campus universitaire, 2092 El Manar Tunis, Tunisia
[b] Université catholique de Louvain, Institute of Condensed Matter and Nanosciences (IMCN), Division MOlecules, Solids and ReactiviTy (MOST), Croix du Sud 2/17, B-1348 Louvain-la-Neuve, Belgium

ARTICLE INFO

Article history:
Received 15 June 2011
Received in revised form 29 July 2011
Accepted 1 August 2011
Available online xxxx

Keywords:
Sol–gel
Aerogel
Sulfate
Vanadia–titania
Oxidation of chlorobenzene

ABSTRACT

This paper examines the effect of sulfation of aerogel vanadia–titania catalysts prepared by sol–gel route on its activity in the total oxidation of chlorobenzene. The catalysts have been characterized by means of ICP-AES, N_2 physisorption, XRD, Raman spectroscopy, XPS, H_2-TPR and NH_3–TPD. This study demonstrated that the VTiS ternary catalyst exhibits higher activity compared to binary VTi. This result could be explained by the fact that sulfate species improves the acidity of the solid and hence ensures that vanadium species are in a high oxidation state leading to a better activity of sulfated catalyst.

1. Introduction

In recent years, high concerns have been raised about atmospheric environmentally hazardous wastes [1]. In particular, the release of chlorinated volatile organic compounds (Cl-VOCs) has received much attention due to the major health problems associated with the exposure to these compounds [2,3]. Many methods have been applied to destroy chlorinated VOCs. Among these, supported vanadium oxide is reported as a very active catalyst resistant against chlorine poisoning [2,4,5]. The enhanced activity of supported vanadia is generally considered to result from an interaction between the support and the vanadium oxide at the interface [6]. The amount of vanadia oxide is fixed to be small due to the requirement in the industrial practice to limit the oxidation of SO_2 to SO_3 as much as possible in the case of the elimination of Cl-VOCs from sulfur bearing fuels [7,8].

Many supports like Al_2O_3, SiO_2 and TiO_2 have been used [9,10]. However, TiO_2 anatase, as a support for the V_2O_5 active phase, is receiving great attention due to its good mechanical, thermal, and anticorrosive properties [10]. The major problem associated with TiO_2 supported catalysts is the phase transformation of anatase to rutile, which involves a decrease in cell volume, an increase in density, mechanical strains and a reduction in surface area leading to an overall degradation of the quality of the catalyst [11]. Indeed, synthesizing anatase TiO_2 with high surface area is a key in the development of efficient catalysts. In addition, sulfated titania was already shown to be a more efficient support [2,12–14]. The reason for doping catalysts by SO_4^{2-} is to provide highly acidic solids [15]. In fact, the acidity of a catalyst could play a crucial role in the adsorption of the VOCs on its surface [2,16]. The enhanced performances of the catalysts prepared with TiO_2/SO_4^{2-} as support are due to (i) their Brønsted acidity which promotes the adsorption of the aromatics on the acid sites of the support and (ii) strong Lewis sites which improve the spreading of the VO_x phase [2,10,17,18]. Many factors may influence the formation of acid sites, such as the preparation method, the sulfate content and the calcination temperature [19].

In this paper, pure anatase TiO_2 powders, as well as V_2O_5–TiO_2 and V_2O_5–TiO_2/SO_4^{2-} catalysts are synthesized by a one step sol–gel method. In order to obtain highly porous materials, the gels were transformed into aerogels using a supercritical drying process. The structural, acidic and redox properties of all catalysts have been characterized by XRD, ICP-AES, N_2 physisorption, XPS, H_2-TPR, Raman spectroscopy and NH_3–TPD. A tentative correlation with the activity in total oxidation of chlorobenzene is established and the effect of the addition of SO_4^{2-} is discussed. The direct incorporation of sulfate species in the support was investigated.

2. Experimental

2.1. Sample preparation

The synthesis of TiO_2 supports was carried out as follows: first, titanium (IV) isopropoxide as precursor with anhydrous ethanol as

* Corresponding author. Tel.: +216 96 940 755.
E-mail address: gannoun.chiraz@gmail.com (C. Gannoun).

1566-7367/$ – see front matter
doi:10.1016/j.catcom.2011.08.001

solvent was chemically modified by adding acetylacetone to control hydrolysis and condensation reaction rates. A homogeneous gel is then obtained after HNO_3 supply. Water is added according to the molar ratio $h = H_2O/Ti$ equal to 5, 7.5 and 10 in order to investigate the effect of the hydrolysis ratio on the surface area of TiO_2. Mixed vanadia oxide (V_2O_5–TiO_2) catalyst is prepared with $h = 10$ by adding vanadyl acetylacetonate to the organic mixture with a theoretical amount of vanadia loading (2 wt.%) and stirred for 1 h; this sample is called VTi. To obtain sulfated oxides, concentrated sulfuric acid is added according to the molar ratios $S/Ti = 0.1$ and 0.2. The samples are called respectively VTiS1 and VTiS2. The gels were, thereafter, transformed into aerogels by supercritical drying ($P = 63$ bar, $T = 243$ °C). The obtained aerogels were then calcined for 12 h at 500 °C under O_2 flow (30 ml/min).

2.2. Characterization

Specific surface area and pore volume measurements of the samples were done by N_2 physisorption at 77 K using a Micromeritics ASAP 2000 apparatus. The samples were outgassed in vacuum during 6 h at 200 °C prior the nitrogen physisorption.

X-ray diffraction patterns (XRD) were obtained using a MRD PRO PANalytical X'Pert PRO instrument with Cu Kα radiation ($\lambda = 1.5418$ Å) at the rate of 0.02°/s from 5 to 70 °C.

Total acidity was evaluated by temperature-programmed desorption of ammonia (TPD/NH_3) using a quadrupole Balzers QMC 311. Before NH_3 desorption, the samples were pre-treated under He flow (60 ml/min) at 200 °C for 1 h. NH_3 adsorption was performed under ambient conditions by flowing 0.5% NH_3 in He over the catalyst until saturation and then desorption of physisorbed NH_3 by temperature-programmed treatment under He from 50 to 550 °C using a heating rate of 10 °C/min.

Temperature programmed reduction (TPR) experiments were performed in a dynamic apparatus using 5% H_2 in helium as a balance gas flowing at 60 ml/min. Experiments were carried out in the range 30–800 °C. The inlet and the outlet gas composition were measured using a quadrupole mass spectrometer QMC 311 Balzers coupled to the reactor.

X-ray photoelectron spectra (XPS) were performed on a SSI X probe spectrometer (model SSI 100, Surface Science Laboratories, Mountain View, CA) equipped with a monochromatized Al-Kα radiation (1486 eV). The sample powders, pressed in small stainless troughs of 4 mm diameter, were placed on an insulating home-made ceramic carousel. The pressure in the analysis chamber was around 10^{-6} Pa. The analyzed area was approximately 1.4 mm^2 and the pass energy was set at 150 eV. The C1s peak of carbon has been fixed to 284.8 eV to set the binding energy scale. Data treatment was performed with the CasaXPS program (Casa Software Ltd, UK) and some spectra were decomposed with the least squares fitting routine provided by the software with a Gaussian/Lorentzian (85/15) product function and after subtraction of a nonlinear baseline.

The elemental analysis was performed by inductively coupled plasma-atomic emission spectroscopy (ICP-AES) allowing estimating the weight percentage of S and V. These measurements were performed on an Iris Advantage apparatus from Jarrell Ash Corporation.

Raman spectra were measured with a Dilor Instrument S.A. spectrometer with the 632 nm line of Ar ion laser as excitation source under ambient conditions. The number of scans is 10 and the time of accumulation is 10 s per scan.

2.3. Catalytic tests

Catalytic tests were performed with 200 mg of catalyst (200–315 μm) diluted in 800 mg of inactive glass spheres with diameters in the range 315–500 μm in a metallic fixed-bed micro-reactor (PID Eng&Tech, Madrid, Spain) operating at atmospheric pressure and fully monitored by a computer. The gas stream was composed of 100 ppm of chlorobenzene, 20 vol.% of O_2 and helium as diluting gas to obtain 200 ml/min (space velocity (VVH) = 37,000 h^{-1}). The reaction was run from 100 to 400 °C in a step mode with a 150 min plateau at each temperature investigated. Analysis of reactants and products was continuously performed by on line gas chromatography (GC). The GC allowed to quantify chlorobenzene, O_2, CO, and CO_2 and to detect other hydrocarbons and halocarbons. At each temperature increase, a transient period (typically 30–50 min) is observed during which CO_2/CO production is slightly higher than chlorobenzene conversion. This is attributed to the combustion of organic matter deposited during the tests at the lowest temperatures (unreactive adsorption). Thus, to calculate the conversion, only the concentrations of reactants and products measured after stabilization and averaged in the period of time from 100 to 150 min were taken into account. The measured performances were accurate within a range of about 1% (in relative) for the conversion of chlorobenzene.

3. Results and discussion

BET specific surface areas and mean pore size diameters of the TiO_2 supports prepared with different hydrolysis molar ratios ($h = H_2O/Ti =$ 5, 7.5 and 10) and calcined at 500 °C are shown in Table 1. All solids are classified as mesoporous materials (pores between 20 and 500 Å) and exhibited comparable surface areas which are higher than industrial TiO_2 such as TiO_2 Degussa p-25, which is a mixture of anatase (70%) and rutile (30%) and which has a surface area of 50 m^2/g [20]. However, the support prepared with $h = 10$ presents the best homogeneous and monomodal porous distribution. Consequently, vanadia supported TiO_2 catalysts are prepared with a hydrolysis molar ratio equal to 10.

The X-ray diffraction patterns for the three TiO_2 supports treated at 500 °C show only the diffraction lines of the anatase phase such as $2\theta = 25°$, 23°, 37°, 48° and 53°. No rutile phase was detected in these oxides (Fig. 1). This result is very promising since commercial TiO_2 failed to provide TiO_2 in a form of anatase with high surface area.

Theoretical and experimental chemical compositions of the investigated samples VTi, VTiS1 and VTiS2 are compared in Table 2. The results indicate that vanadium was successfully incorporated in the catalysts. For sulfated samples, differences between the theoretical and the obtained sulfur rate could be attributed to calcination. In fact, treating catalysts at high temperature and under oxidant atmosphere could be responsible for the loss of some of the sulfur.

BET specific surface areas and porous diameters of the catalysts calcined at 500 °C are listed in Table 3. All solids are mesoporous and exhibit similar surface areas. In the literature, it is usually reported that in V_2O_5/TiO_2 systems the surface area decreases with the V_2O_5 content [12]. However, in this work, the VTi sample containing 2 wt.% V_2O_5, was found to display a greater surface area (135 m^2/g instead of 115 m^2/g). In addition, it is clear that the presence of sulfate groups does not change the surface areas. Therefore, we can rule out a possible surface area effect when comparing the physico-chemical and activity properties of the sulfated and unsulfated samples.

The XRD patterns for samples treated at 500 °C show only the diffraction lines of the anatase phase (figure not shown). No diffraction peaks due to crystalline vanadia oxide were detected, indicating that V_2O_5 species were highly dispersed over TiO_2 and TiO_2/SO_4^{2-} supports.

Table 1
Specific surface area and mean pore size diameter of TiO_2 support prepared with different hydrolysis molar ratios and calcined at 500 °C.

$h = H_2O/Ti$	Surface area (m^2/g)	Pore diameter (Å)
10	115	80
7.5	109	117
5	106	190

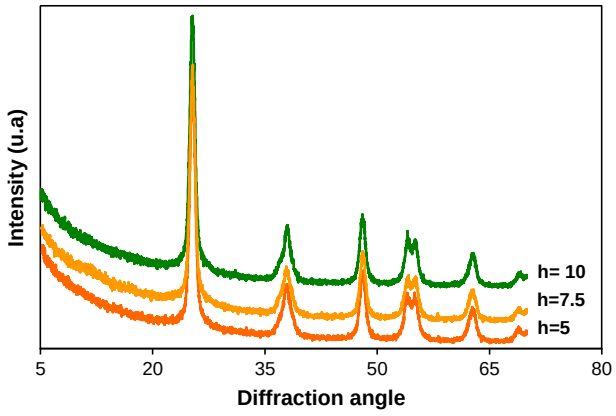

Fig. 1. X-ray diffraction patterns of TiO_2 supports prepared with different hydrolysis molar ratios.

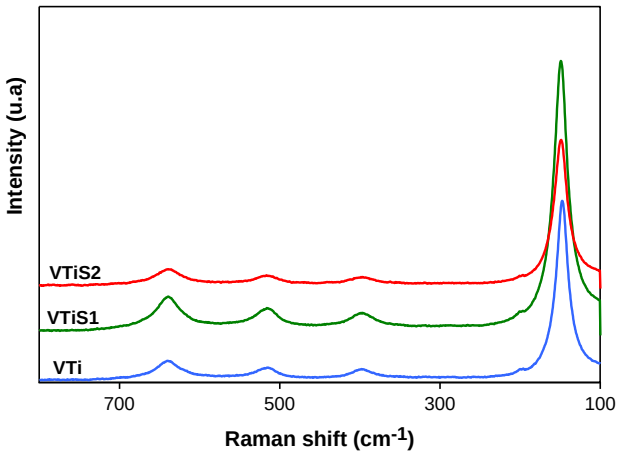

Fig. 2. Raman spectra of VTi and VTiS catalysts treated at 500 °C.

These results are in perfect accordance with the obtained Raman spectra. In fact, as shown in Fig. 2, the bands at 150, 401, 520 and 645 cm^{-1} belonging to anatase phase were observed for all samples [21]. No bands were observed at the Raman shifts of 1030 and 900–1000 cm^{-1} representing the terminal V═O bond of monomeric vanadyl and polymeric vanadate species, respectively [22,23]. Besides, it was reported in the literature [24] that the sulfate species present on sulfated V_2O_5/TiO_2 samples display a characteristic band around 1370 cm^{-1} in the Raman spectra due to terminal S═O bonds. However, this band was not observed for our VTiS likely due to the low content of sulfate incorporated in our catalysts.

Table 4 summarizes the XPS binding energies of O, Ti, S and V present on the surface of the samples. The binding energies of Ti $2p_{3/2}$ for all catalysts were around 459 eV, characteristic of Ti^{4+} [24,25]. This oxidation state remains unchanged for sulfated and unsulfated catalysts. A contribution with binding energies around 515 and 517 eV was detected for all samples containing vanadia, suggesting that vanadium, in this study, consists in a mixture of IV and V oxidation states [26]. The common main peaks of O 1s for all the catalysts were around 530 eV, which is typical of oxide oxygen. For sulfated catalysts, a peak with a binding energy near 169 eV was measured for the S 2p. According to literature, such an XPS band represents the existence of sulfate on the catalyst surface [24,27,28]. As expected, XPS peaks at 161–162.2 eV (sulfide) or 164 eV (elemental sulfur) are never detected.

Table 5 illustrates XPS surface contents in vanadium and sulfur. The comparison between bulk (Table 2) and surface contents (Table 5) shows that vanadium content in VTi sample is the same everywhere in the catalyst. The understanding of the VTiS catalyst results is more complex and has to consider the presence of sulfur. Indeed, XPS suggests that there is less vanadium at the surface of VTiS catalysts than at the surface of VTi sample. However, this comparison is not relevant because it does not consider that the presence of superficial sulfate groups decreases the relative exposure of vanadium at the surface of the catalysts. The presence of sulfate groups thus influences directly the relative surface content of vanadium and impedes a direct comparison with VTi catalyst. However, the calculation of the bulk and the surface vanadium contents in VTiS catalysts without considering sulfur shows a higher V content in the bulk than at the surface. Indeed, the bulk vanadium contents correspond to 1 and 0.96% respectively for VTiS1 and VTiS2 while the surface vanadium contents are 0.73 and 0.80%. At the opposite, the analysis of the bulk and the surface sulfur contents shows that the surface sulfur contents are higher than in the bulk, indicating that the sulfate ions mainly exist on the surface of VTiS catalysts.

Fig. 3 presents the chlorobenzene oxidation in terms of conversion as a function of the reaction temperature in the range 100–400 °C. CO_2 is the main product. Carbon monoxide is also produced especially at a relatively high temperature (from a few% up to ca. 30%). No other partial oxidation products (chlorinated or not) are observed. These observations hold for all catalysts. The VTi binary system is virtually inactive for chlorobenzene conversion below 300 °C and exhibits a low activity above 350 °C (conversion is only about 30% at 400 °C).

Table 2
Element analysis and theoretical composition of "sulfated and unsulfated catalysts calcined at 500 °C.

Catalyst	Bulk composition (wt.%)		Theoretical composition (wt.%)	
	V	S	V	S
VTi	1.07	–	1.1	–
VTiS1	0.98	2.01	1.1	4%
VTiS2	0.94	2.25	1.1	8%

Table 3
Specific surface area and mean pore size diameter of sulfated and unsulfated catalysts calcined at 500 °C.

Catalyst	Surface area (m^2/g)	Pore diameter (Å)
VTi	135	83
VTiS1	135	56
VTiS2	137	71

Table 4
XPS binding energies of VTi, VTiS1 and VTiS2 catalysts.

Catalyst	Binding energy (eV)				
	O 1s	Ti $2p_{3/2}$	V $2p^{5+}_{3/2}$	V $2p^{4+}_{3/2}$	S 2p
VTi	529.8	458.6	517.1	515.9	–
VTiS1	530.2	459.0	517.3	515.8	168.9
VTiS2	530.3	459.1	517.1	515.7	168.9

Table 5
Surface composition of VTi, VTiS1 and VTiS2 calculated from XPS data.

Catalyst	Surface composition (wt.%)	
	V[a]	S
VTi	1.1	–
VTiS1	0.70	4.2
VTiS2	0.77	4.6

[a] Vanadium composition is calculated from XPS data without considering sulfate in the calculation of weight percentages.

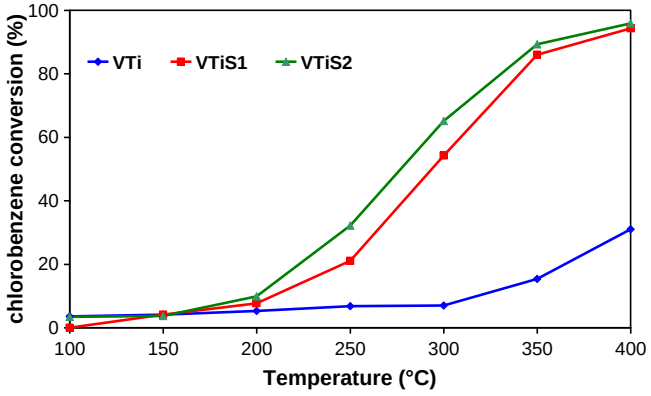

Fig. 3. Chlorobenzene conversion over vanadia supported catalysts.

The corresponding sulfated catalysts are considerably more active, reaching 94 and 96%, respectively, for VTiS1 and VTiS2 at 400 °C. It can be noted as well that the transient period classically observed at each temperature rise (see Experimental section) is shorter for sulfate-containing catalysts. This indicates that the unproductive adsorption is less significant, or in other words, that the oxidation potential is more pronounced on the latter catalysts. These observations point out the beneficial role of sulfate groups on the catalytic activity of V_2O_5–TiO_2 aerogel catalysts on chlorobenzene oxidation.

To evaluate the effect of sulfate ion in this system, NH_3–TPD experiments were carried out. The results are shown in Fig. 4. A reference sulfated support was prepared with a molar ratio S/Ti = 0.2 following the synthesis described above but without V in the preparation. As seen in Fig. 4A, the NH_3 desorption spectrum of unsulfated titania shows two unresolved peaks at around 100 °C and 350 °C which can be attributed to NH_3 desorbed from weak and strong acidic sites, respectively [29–31]. The sulfation of the support increases the intensity of the peak around 100 °C and shifts the peak around 350 °C to 430 °C, indicating that the presence of the sulfate groups in TiO_2 support significantly enhances the total acidity of the TiO_2 material. For VTi catalyst, the intensity of the first peak (100 °C) increases considerably whereas strong acidic sites remain almost constant. These observations suggest that weak acid sites are present on the surface of V_2O_5 phase but almost not on the surface of the support. For VTiS samples, weak acidic sites further increase, along with a slight decrease of strong acidic sites (Fig. 4B) suggesting a progressive transformation of the surface acidity due to the strong interaction between sulfate groups and vanadia species. It seems that the vanadium–sulfate interaction created new weak acidic sites bringing about an enhancement of performances as discussed in earlier investigations [2,18,32]. Based on this hypothesis, we can understand, now, why our VTiS1 and VTiS2 catalysts show little difference in their catalytic activity since their amount of superficial sulfate groups is only slightly different as shown by XPS measurements.

In order to evaluate the redox properties of metal oxide catalysts, H_2-TPR measurements were carried out (Fig. 5). For TiO_2 support, no H_2 peak consumption was observed (Fig. 5A). However, for the sulfated solids, the hydrogen consumption began at 500 °C and two peaks appeared at around 639 and 650 °C assigned to the reduction of sulfate species into SO_2 essentially as observed in earlier works [13,31,32]. After vanadium incorporation, the TPR profile of the unsulfated catalyst exhibits a weak peak centered at about 446 °C which might be ascribed to the reduction of VO_x species [33,34]. However, the presence of vanadium at the surface of sulfated catalysts affects the reduction behavior of sulfate groups. Especially, the reducibility of sulfate becomes more important in the ternary solid

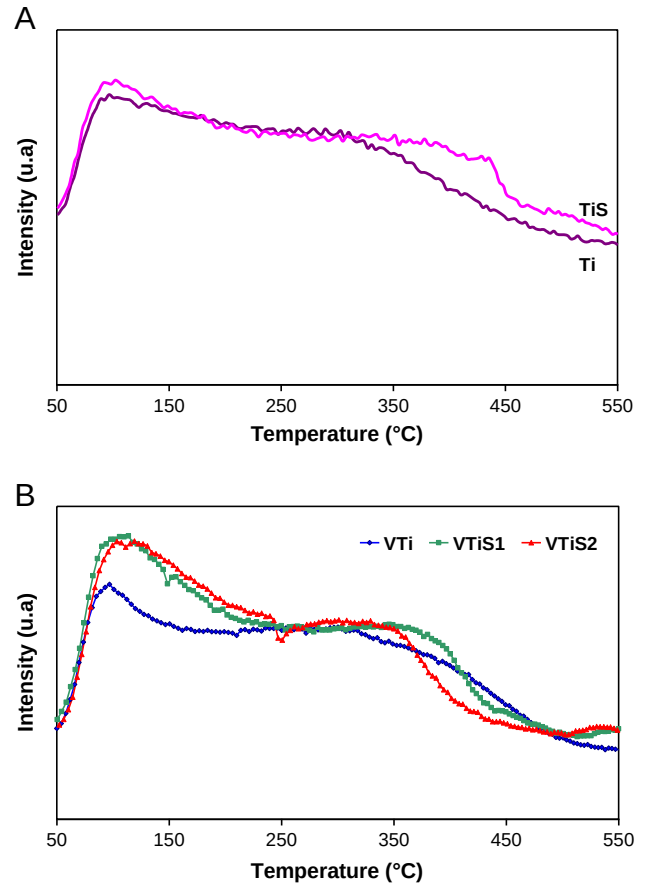

Fig. 4. NH_3–TPD profiles of the samples treated at 500 °C: (A) Ti and TiS supports, (B): VTi, VTiS1 and VTiS2 catalysts.

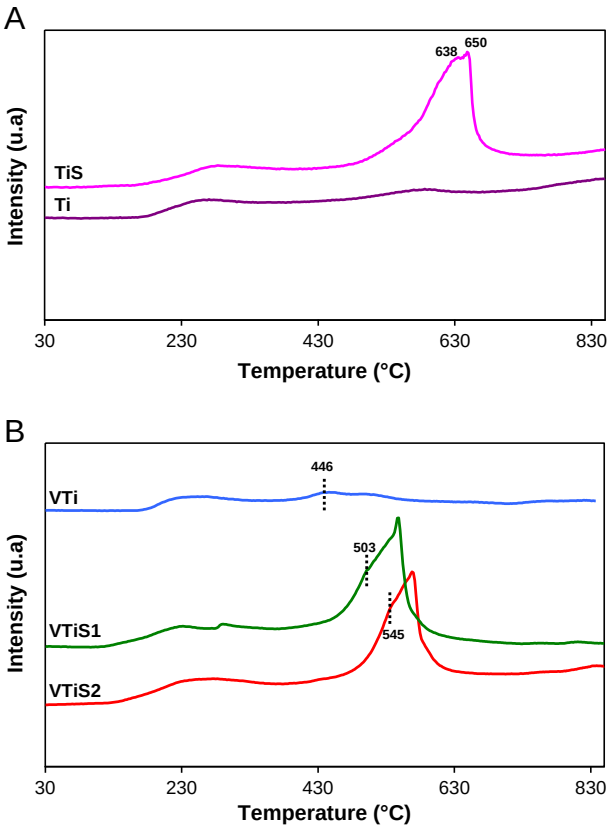

Fig. 5. H_2-TPR profiles of the samples treated at 500 °C : (A) Ti and TiS supports, (B) VTi, VTiS1 and VTiS2 catalysts.

Table 6
Specific surface areas of the tested sulfated and unsulfated catalysts.

Tested catalysts	Surface area (m^2/g)
VTi	93
VTiS1	95
VTiS2	95

(VTiS) than in the binary one (TiS) since TPR reduction peaks shifted toward lower temperature (Fig. 5B). These observations highlight the interaction between vanadium and sulfate groups. It seems that this interaction enhances the reducibility of VTiS materials and improves the reactivity of vanadium redox sites for the chlorobenzene oxidation. A similar result was reported by Arfaoui et al. using VTi-Pillared Clays and VTiS-Pillared Clays in the epoxidation of allylic alcohol [32]. Moreover, it appears that the introduction of SO_4^{2-} succeeds to stabilize the vanadium in a higher oxidation state. In fact, the incorporation of SO_4^{2-} is observed by H_2-TPR to slightly inhibit the reduction of vanadia since the vanadium reduction peak maxima at 446 °C slightly shifted to higher temperatures (shoulder at 503 and 545 °C for VTiS samples).

It is quite obvious that there is an intimate parallelism between the efficiency of the sulfated catalysts and the fact that they are operated with their V_2O_5 phase maintained, thanks to sulfates, in a high oxidation state. Although vanadium is more exposed on the surface of unsulfated catalyst as shown by XPS results (Table 5), the low reducibility of vanadium on the surface of sulfated catalysts leads to a better catalytic activity. These results are consistent with a catalytic mechanism proceeding in four steps: i) adsorption of chlorobenzene on weak (likely "Brønsted") acid sites, ii) V_2O_5 redox sites give some of their oxygen atoms to oxidize the aromatic ring producing H_2O and CO_2, iii) reoxidation of the V_2O_5 reduced sites thanks to the gas stream oxidant (O_2) and iv) retrieving of the chlorine from the surface, as already suggested in previous works [2,18]. The second and third steps compose a classical Mars and van Krevelen mechanism [35].

In order to investigate the stability of our catalysts, prolonged catalytic tests were carried out over a 10 hour-period at 300 °C. A deactivation of about 24% in chlorobenzene oxidation has been observed on the most active catalyst (VTiS2). This phenomenon could be explained by the deposition of the coke at the surface of the pores. The specific surface area loss observed on the tested catalysts confirmed this hypothesis (Table 6). On the other hand, the XRD characterization of these catalysts indicates a stability of the crystalline phases. In fact, no formation of V_2O_5 and no collapse of the anatase structure have been observed (XRD patterns not shown).

4. Conclusion

This research has mainly demonstrated that sulfate containing Vanadia–titania aerogel catalysts prepared via sol–gel method considerably improved catalytic properties in the chlorobenzene oxidation at high temperature as compared to corresponding unsulfated gels. In fact, sulfate ions affect the properties of oxides in several ways:

- Sulfate groups interact with vanadium species, creating more weak acidic sites which are beneficial for chlorobenzene oxidation at high temperature.
- Sulfation stabilizes the vanadium in a higher oxidation state which correlates with the beneficial effect of sulfate for chlorobenzene conversion.
- The interaction between sulfate groups and vanadium species enhances the reducibility of VTiS material and the reactivity of vanadium redox sites, leading to more active catalysts in chlorobenzene oxidation than the VTi catalyst.

References

[1] C. Jia, S. Batterman, C. Godwin, Atmospheric Environment 42 (2008) 2083–2100.
[2] R. Delaigle, D.P. Debecker, F. Bertinchamps, E.M. Gaigneaux, Topics in Catalysis 52 (2009) 501–516.
[3] E.E. Chang, W.C. Wang, L.X. Zeng, H.L. Chiang, Inhalation Technology 22 (2010) 117–125.
[4] F. Bertinchamps, C. Poleunis, C. Gregoire, P. Eloy, P. Bertrand, E.M. Gaigneaux, Surface and Interface Analysis 40 (2008) 231–236.
[5] D.P. Debecker, R. Delaigle, P. Eloy, E.M. Gaigneaux, Journal of Molecular Catalysis A: Chemical 289 (2008) 38–43.
[6] B. Grzybowska-Swierkosz, Applied Catalysis A: General 157 (1997) 263–310.
[7] L.J. Alemany, F. Berti, G. Busca, G. Ramis, D. Robba, G.P. Toledo, M. Trombetta, Applied Catalysis B: Environmental 10 (1996) 299–311.
[8] L.J. Alemany, L. Lietti, N. Ferlazzo, P. Forzatti, G. Busca, G. Ramis, E. Giamello, F. Bregani, Journal of Catalysis 155 (1995) 117–130.
[9] EUROCAT, Catalysis Today 20 (1994) (complete issue).
[10] F. Bertinchamps, C. Gregoire, E.M. Gaigneaux, Applied Catalysis B: Environmental 66 (2006) 1–9.
[11] V. Ahmed Yasir, P.N. MohanDas, K.K.M. Yussef, International Journal of Inorganic Materials 3 (2001) 593–596.
[12] Q. Sun, Y. Fu, J. Liu, A. Auroux, J. Shen, Applied Catalysis A: General 334 (2008) 26–34.
[13] L. Baraket, A. Ghorbel, P. Grange, Applied Catalysis B: Environmental 72 (2007) 37–43.
[14] H. Zhao, S. Bennici, J. Shen, A. Auroux, Journal of Molecular Catalysis A: Chemical 309 (2009) 28–34.
[15] J.P. Chen, R.T. Yang, Applied Catalysis A: General 80 (1992) 135–148.
[16] M.A. Larrubia, G. Busca, Applied Catalysis B: Environmental 39 (2002) 343–352.
[17] B. Ramachandran, H.L. Greene, S. Chatterjee, Applied Catalysis B: Environmental 8 (1996) 157–182.
[18] F. Bertinchamps, C. Grégoire, E.M. Gaigneaux, Applied Catalysis B: Environmental 66 (2006) 10–22.
[19] L.K. Noda, R.M. de Almeida, N.S. Gonçalves, L.F.D. Probst, O. Sala, Catalysis Today 85 (2003) 69–74.
[20] Degussa Technical Bulletin Pigment Report, 56, 1990, p. 13.
[21] B.M. Reddy, A. Khan, Y. Yamada, T. Kobayashi, S. Loridant, J.C. Volta, The Journal of Physical Chemistry. B 107 (2003) 5162–5167.
[22] G.T. Went, L.J. Leu, A.T. Bell, Journal of Catalysis 134 (1992) 479–491.
[23] M.D. Amiridis, I.E. Wachs, G. Deo, J.M. Jehng, D.S. Kim, Journal of Catalysis 161 (1996) 247–253.
[24] J.P. Chen, R.T. Yang, Journal of Catalysis 139 (1993) 277–288.
[25] J.P. Nogier, M. Delamar, Catalysis Today 20 (1994) 109–123.
[26] V.I. Bukhtiyarov, Catalysis Today 56 (2000) 403–414.
[27] S.T. Choo, Y.G. Lee, I.-S. Nam, S.W. Ham, J.B. Lee, Applied Catalysis A: General 200 (2000) 177–188.
[28] M.H. Kim, L.-S. Nam, Y.G. Kim, Journal of Catalysis 179 (1998) 350–360.
[29] L. Chmielarz, P. Kustrowski, M. Zbroja, W. Lasocha, R. Dziembaj, Catalysis Today 90 (2004) 43–49.
[30] L. Chmielarz, P. Kustrowski, M. Zbroja, W. Lasocha, R. Dziembaj, Applied Catalysis B: Environmental 53 (2004) 47–61.
[31] J. Arfaoui, L. Khalfallah Boudali, A. Ghorbel, G. Delahay, Catalysis Today 142 (2009) 234–239.
[32] J. Arfaoui, L. Khalfallah Boudali, A. Ghorbel, Applied Clay Science 48 (2010) 171–178.
[33] H. Poelman, B.F. Sels, M. Olea, K. Eufinger, J.S. Paul, B. Moens, I. Sack, V. Balcaen, F. Bertinchamps, E.M. Gaigneaux, P.A. Jacobs, G.B. Marin, D. Poelman, R. De Gryse, Journal of Catalysis 245 (2007) 156–172.
[34] G.Y. Popova, T.V. Andrushkevich, E.V. Semionova, Y.A. Chesalov, L.S. Dovlitova, V.A. Rogov, V.N. Parmon, Journal of Molecular Catalysis A: Chemical 283 (2008) 146–152.
[35] P. Mars, D.W. van Krevelen, Chemical Engineering Science 3 (1954) 41–59.